J Mol Neurosci (2015) 55:733–748
DOI 10.1007/s12031-014-0412-6

Short-Term Cuprizone Feeding Verifies *N*-Acetylaspartate Quantification as a Marker of Neurodegeneration

Barbara Maria Krauspe · Wolfgang Dreher · Cordian Beyer · Werner Baumgartner · Bernd Denecke · Katharina Janssen · Claus-Dieter Langhans · Tim Clarner · Markus Kipp

Received: 12 August 2014 / Accepted: 20 August 2014 / Published online: 5 September 2014

Abstract Proton magnetic resonance spectroscopy (1H-MRS) is a quantitative MR imaging technique often used to complement conventional MR imaging with specific metabolic information. A key metabolite is the amino acid derivative *N*-Acetylaspartate (NAA) which is an accepted marker to measure the extent of neurodegeneration in multiple sclerosis (MS) patients. NAA is catabolized by the enzyme aspartoacylase (ASPA) which is predominantly expressed in oligodendrocytes. Since the formation of MS lesions is paralleled by oligodendrocyte loss, NAA might accumulate in the brain, and therefore, the extent of neurodegeneration might be underestimated. In the present study, we used the well-characterized cuprizone model. There, the loss of oligodendrocytes is paralleled by a reduction in ASPA expression and activity as demonstrated by genome-wide gene expression analysis and enzymatic activity assays. Notably, brain levels of NAA were not increased as determined by gas chromatography–mass spectrometry and 1H-MRS. These important findings underpin the reliability of NAA quantification as a valid marker for the paraclinical determination of the extent of neurodegeneration, even under conditions of oligodendrocyte loss in which impaired metabolization of NAA is expected. Future studies have to reveal whether other enzymes are able to metabolize NAA or whether an excess of NAA is cleared by other mechanisms rather than enzymatic metabolism.

Keywords Cuprizone · Aspartoacylase · *N*-Acetylaspartate · Proton magnetic resonance spectroscopy

B. M. Krauspe · C. Beyer · K. Janssen · T. Clarner · M. Kipp (✉)
Institute of Neuroanatomy, Faculty of Medicine, RWTH Aachen University, Wendlingweg 2, 52074 Aachen, Germany
e-mail: mkipp@ukaachen.de

W. Dreher
Department of Chemistry, in-vivo-MR, University of Bremen, Bremen, Germany

W. Baumgartner
Institute of Biomedical Mechatronics, Johannes Kepler University Linz, Linz, Austria

B. Denecke
Interdisciplinary Centre for Clinical Research (IZKF) Aachen, RWTH Aachen University, Aachen, Germany

C.-D. Langhans
Department of General Pediatrics, Division of Inherited Metabolic Disease, University Children's Hospital Heidelberg, 69120 Heidelberg, Germany

Abbreviations

1H-MRS	Proton magnetic resonance spectroscopy
APC	Adenomatous polyposis coli protein
APP	Anti-amyloid precursor protein
ASPA	Aspartoacylase
CC	Corpus callosum
CNS	Central nervous system
CD	Canavan disease
Co	Control
Cuprizone	*bis*-Cyclohexanone oxaldihydrazone
GC/MS	Gas chromatography–mass spectrometry
GFAP	Glial fibrillary acid protein
GM	Gray matter
H.E.	Haematoxylin–eosin
HPRT	Hypoxanthin guanine phosphoribosyltransferase
IBA1	Ionized calcium binding adaptor molecule 1
IHC	Immunohistochemistry
LFB	Luxol Fast Blue
MR	Magnetic resonance
MS	Multiple sclerosis
MRI	Conventional magnetic resonance imaging
NAA	*N*-Acetylaspartate

NAWM	Normal-appearing white matter
NAGM	Normal-appearing grey matter
PAS	Periodic Acid Schiff
Real-time RT-PCR	Real-time reverse transcriptase-polymerase chain reaction

Introduction

Multiple sclerosis (MS), a chronic inflammatory and demyelinating disease, was first identified as a distinct neurological disorder by the French neurologist Jean-Martin Charcot and is the most common inflammatory condition of the central nervous system (CNS) in young adults. Despite tremendous research efforts, the etiology of the disease is currently unknown, and its pathogenesis is still only partly understood. Complex genetic traits as well as environmental factors appear to determine the susceptibility to develop the disease. The peripheral activation of auto-reactive T cells targeting myelin proteins has been hypothesized as a key process in disease development. Furthermore, the involvement of diverse humoral (antibodies and complement) and cellular mechanisms, such as primary oligodendroglia degeneration, has been proposed to be involved in MS lesion formation and progression.

The architecture of an active MS lesion is highly complex. The characteristic features of MS lesions are demyelination, oligodendrocyte loss, activation of brain resident inflammatory cells (i.e. microglia and astrocytes) as well as peripheral cell recruitment. Despite this inflammatory aspect, brains of MS patients clearly display neurodegeneration. Axonal damage was already recognized by Charcot, and it is nowadays well understood that axonal damage and loss are key features of MS pathogenesis that correlate with permanent neurological deficits in MS patients (Stadelmann, 2011). Furthermore, although the mechanisms leading to axonal damage are not yet fully understood, it has become increasingly clear that axonal/neuronal loss and dysfunction, respectively, can occur very early in the disease course (De Stefano et al., 2001; Ferguson et al., 1997). In consequence, there is a broad consensus that novel treatment options which combine neuroprotection with anti-inflammatory effects are needed.

Conventional magnetic resonance imaging (MRI) techniques are widely applied to monitor the disease natural progression history and its modification by treatment. However, serial studies of lesion measures have often yielded disappointing correlations with the development of clinical disability. A potential explanation for this is the presence of abnormalities, beyond the visible lesions, in the so-called normal-appearing white matter (NAWM) and grey matter (NAGM) (Kirov et al., 2013; Lund et al., 2013; Mistry et al., 2014). Proton magnetic resonance spectroscopy (1H-MRS) can provide additional information to conventional MRI when studying subtle changes in brain tissues. 1H-MRS may detect signs of axonal damage in what appears to be normal white and grey matter and allows for absolute quantification of specific metabolites. Consequently, 1H-MRS is often used to provide specific biochemical information via the levels of several detectable neurometabolites.

Of these, the amino acid derivative *N*-Acetylaspartate (NAA), first described by Tallan et al. in 1956 (Tallan et al., 1956), is almost exclusively attributed to neurons and their processes in the brain (Moffett et al., 1991; Simmons et al., 1991). Because, after glutamate, it is the second most abundant amino acid in the human central nervous system (CNS) (NAA comprises up to 0.1 % wet weight of the brain), its single peak is the most intense in 1H-MRS of a healthy brain (Rigotti et al., 2007). Reduced levels of NAA indicate axonal degeneration or axonal loss in white matter lesions or neuronal damage distant from the areas of investigation (Bitsch et al., 1999). Indeed the neuronal compound NAA, as measured by 1H-MRS, is currently the best and most specific non-invasive marker of neuronal and axonal pathology in MS patients (Bjartmar et al., 2000; Bjartmar et al., 2002).

NAA is synthesized in the brain through acetylation by acetyl coenzyme A of free aspartate by the enzyme L-aspartate *N*-acetyltransferase and catabolized by the enzyme aspartoacylase (ASPA) (Goldstein, 1959). In the case of Canavan disease (CD), it was found that a mutation in the gene for the enzyme ASPA resulted in an inability to catabolize NAA, leading to a progressive, fatal leukodystrophy in affected individuals (Moffett et al., 2007). High levels of NAA were detected in the brains of many CD patients who lacked the degrading enzyme ASPA, suggesting that an excess of NAA levels may have detrimental effects in the CNS. During NAA catabolism, NAA is transported from neurons to the cytoplasm of oligodendrocytes, where ASPA cleaves the acetate moiety for use in fatty acid and steroid synthesis (Madhavarao et al., 2002; Mattan et al., 2010). It is assumed that the fatty acids and steroids produced are then used as building blocks for myelin lipid synthesis (Moffett et al., 2007).

Several studies reported reduced NAA levels in the NAWM of MS patients, mirroring neuronal/axonal damage (Gustafsson et al., 2007; Wattjes et al., 2008). In line with this assumption, clinical disability has been correlated with reduced NAA in both cerebral (Davie et al., 1997; Sarchielli et al., 1999) and cerebellar (Davie et al., 1995) NAWM. Other studies, however, were not able to detect any changes of NAWM NAA levels between MS patients and control subjects (Fernando et al., 2004; Vrenken et al., 2005). Since NAA is metabolized by oligodendrocytes, we aimed to determine whether NAA accumulates in the brain of animals during early cuprizone administration. In this model, early and widespread oligodendrocyte dysfunction is spatio-temporally followed by oligodendrocyte apoptosis (Acs et al., 2013;

Buschmann et al., 2012; Kipp et al., 2009; Skripuletz et al., 2011). In consequence, NAA catabolism might be disturbed, leading to a "masking" of neuronal/axonal degeneration in MS tissues.

Materials and Methods

Animals and Induction of Demyelination

C57BL/6 male mice (Harlan Winkelmann, Germany) were bred and maintained in a pathogen-free environment. The animals underwent routine cage maintenance once a week and microbiological monitoring according to the Federation of European Laboratory Animal Science Associations recommendations. Food and water were available ad libitum. Research and animal care procedures were formally approved by the Review Boards for the Care of Animal Subjects of the district government (North Rhine-Westphalia, Germany and Bremen, Germany). Oligodendrocyte pathology was induced by feeding 8-week-old (19–21 g) male mice a diet containing 0.2 % cuprizone (*bis*-cyclohexanone oxaldihydrazone; Sigma–Aldrich Inc., USA) mixed into a ground standard rodent chow for the indicated period. ASPA$^{Nur7/Nur7}$ mice were purchased from Jackson laboratories and genotyped as published previously (Clarner et al., 2013).

Tissue and Sample Preparation

Tissue preparation was performed as previously described (Clarner et al., 2012; Kipp et al., 2011a). For histological and immunohistochemical studies, mice were transcardially perfused with ice-cold PBS followed by transcardial perfusion with 4 % paraformaldehyde solution containing picric acid (pH 7.4). After overnight post-fixation in the same fixative, brains were dissected, embedded, and then coronary sectioned into 5-μm sections at the levels 205–285 according to the mouse brain atlas by Sidman et al. (http://www.hms.harvard.edu/research/brain/atlas.html). For gene expression studies, NAA level quantification, and enzymatic activity assays, tissues were dissected after 0.9 % NaCl perfusion, immediately frozen in liquid nitrogen, and kept at −80 °C until use.

Gene Expression Analysis

Gene expression levels were measured using the rt RT-PCR technology (BioRad, Germany), SensiMix Plus SYBR and Fluorescein (Quantace, Germany), and a standardized protocol as described previously by our group (Buschmann et al., 2012; Clarner et al., 2012). Primer sequences and individual annealing temperatures are shown in Table 1. Relative quantification was performed using the ΔΔCt method which results in ratios between target genes and the housekeeping reference gene hypoxanthine guanine phosphoribosyltransferase (HPRT). Melting curves and gel electrophoreses of the PCR products were routinely performed to verify the specificity of the PCR reaction (data not shown).

Gene Array Analysis

Gene expression in different treatment groups was analyzed using the GeneChip® Mouse Gene 1.0 ST Array (Affymetrix, Santa Clara, CA, USA) in independent triplicates as published previously (Johann et al., 2008; Kipp et al., 2008; Kipp et al., 2011a). Total RNA was isolated and quantified (Nanodrop). RNA quality was assessed using RNA 6000 Nano Assay with the Agilent 2100 Bioanalyzer (Agilent, Santa Clara, CA, USA). Probes for the GeneChip® Mouse Gene 1.0 ST arrays were prepared and hybridized to the arrays according to the Ambion whole-transcript expression and the Affymetrix whole-transcript terminal labeling and control kit manuals. Briefly, for each sample, 300 ng of total RNA was reverse-transcribed into cDNA using a random hexamer oligonucleotide tagged with a T7 promoter sequence. After second strand synthesis, double-stranded cDNA was used as a template for amplification with T7 RNA polymerase to obtain antisense cRNA. Random hexamers were then used to reverse-transcribe the cRNA into single-stranded sense strand cDNA. The cDNA was then fragmented by uracil DNA glycosylase and apurinic/apyrimidic endonuclease 1. Fragment size was checked using the Agilent 2100 Bioanalyzer (fragment size between 50 and 200 bp). Fragmented sense cDNA was biotin-endlabelled with TdT and probes were hybridized to the GeneChip® Mouse Gen 1.0 ST arrays at 45 °C for 16 h. Hybridized arrays were then washed and stained on a Fluidics Station 450 and scanned on a GeneChip® Scanner 3000 7G (both Affymetrix).

Table 1 Sequences of primers used in the study

Gene	Sense	Antisense	Length (bp)
ASPA	aca tgg ctg ctg tta ttc atc c	ggg tac acg gta cag tct cca	127
GFAP	gag atg atg gag ctc aat gac c	ctg gat ctc ctc ctc cag cga	380
HPRT	gct ggt gaa aag gac ctc t	cac agg act aga aca cct gc	248

Raw image data were analyzed with AGCC (Affymetrix, USA), and gene expression intensities were normalized and summarized with robust multiarray average algorithm (Irizarry et al., 2003). Only genes expressed more than three-fold compared to array internal negative controls were taken into further consideration. Transcripts lower expressed in the 2 days cuprizone-treated group in comparison to the control group with an adjusted *p*-value of less than 0.05 were considered as down-regulated.

Immunohistochemistry and Histochemical Analysis

For immunohistochemistry (IHC), sections were rehydrated, and if necessary, epitopes were unmasked by Tris/EDTA-buffer (pH 9.0) or citrate buffer (pH 6.0) heating, washed in PBS, and incubated overnight (4 °C) with the primary antibody diluted in blocking solution (serum of species in which the secondary antibody was raised). Anti-adenomatous polyposis coli protein (APC 1:100, mouse IgG; Calbiochem, Germany) antibody was used to detect mature oligodendrocyte cell bodies, anti-glial fibrillary acidic protein (GFAP, 1:12,000, EnCor Biotechnologie, Inc.) antibody was used to visualize astrocytes, anti-ionized calcium-binding adaptor molecule-1 (IBA-1, 1:10,000, Wako Chemicals GmbH) antibody was used to detect microglia/macrophages, and anti-amyloid precursor protein (APP, 1:5000, Merck Millipore) antibody was used to detect acute axonal damage. The next day, slides were subsequently incubated with biotinylated secondary antibodies for 1 h, followed by peroxidase-coupled avidin–biotin complex (ABC kit, Vector Laboratories, UK), and treated with 3,3-diaminobenzidin (DAKO, Germany) as a peroxidase substrate.

Luxol Fast Blue (LFB)/ Periodic Acid Schiff (PAS) stains were performed following established protocols (Acs et al., 2009). Stained and processed sections were digitalized using Nikon ECLIPSE E200 microscope (Nikon, Germany) equipped with a DS-Vi1 camera.

Western Blotting

Western blotting was performed as described previously (Kipp et al., 2011a). Briefly, proteins were isolated with the NucleoSpin RNA/protein kit (Macherey-Nagel, Germany), and 3 μg of entire protein was separated by 10 % SDS–PAGE, blotted semi-dry onto nitrocellulose membranes (Amersham™ Hybond™-ECL, GE Healthcare, UK), blocked, and incubated with primary antibodies diluted in 5 % milk TBS–Tween 0.01 % overnight (anti-β-Actin, Sigma, USA, 1:1,000, 42 kDa or anti-GFAP, EnCor, USA, 1:10,000, 55 kDa). After washing and incubating with horseradish peroxidase conjugated secondary antibodies (Bio-Rad Laboratories, Inc., USA), labeled proteins were visualized with ECL-reagent. Visualization of β-actin levels using the indicated antibodies was used as loading control.

Electron Microscopy

Electron microscopy was performed as published previously (Norkute et al., 2009; Pott et al., 2009). In brief, mice were perfused with a buffer containing 100 mM cacodylate, pH 7.2, (Fluka, Germany), 1.5 % (v/v) formaldehyde (AppliChem, Germany), 1.5 % glutaraldehyde (Fluka, Germany), and 5.8 g/l NaCl. Trimmed brain sections were post-fixed for 1 h in 1 % (*w*/*v*) OsO_4 (Fluka, Germany) in PBS, dehydrated, and embedded in Epon 812 (Epon mix, Serva, Germany). Thin sections were cut, contrasted with uranyl acetate and lead citrate, and myelination of axons was analyzed with a Zeiss EM10C electron microscope.

Aspartoacylase Activity Assay

The ASPA activity measurement was performed as published elsewhere (Bhakoo et al., 2001) with modification of the applied NAA concentration which was adjusted from 2 to 10 mM due to the enzyme kinetics (V_{max}=0.1964 nmol/min). The amount of protein used was about 350 μg per tissue sample. Briefly, snap-frozen cortices were homogenized in $CaCl_2$ with Precelly® homogenizer system (PEQLAB Biotechnologie GMBH, Germany). After sonication, Triton X-100 (0.04 % final concentration) was added. Tissue lysate was subsequently incubated with NAA (10 mM) for 2 h at 37 °C. To stop the hydrolyzation of NAA to aspartate and acetate, probes were incubated for 10 min at 100 °C before the reaction buffer (1.5 mM NADH; 30 mM α- Ketogluterat; MAD; 0.1 M Tris-HCl, pH 8.0) was added. After determination of NADH absorbance at 340 nm in an UVette® (d= 10 mm, Eppendorf AG, Germany) using a BioPhotometer plus (Eppendorf AG, Germany), GOT was added to start the two enzymatic reactions which result in the oxidation of NADH, and probes were incubated for 2 h at 37 °C. Finally, NADH absorbance was measured again. Protein concentration was determined by bicinchoninic acid protein assay (Pierce™ BCA Protein Assay kit, Thermo Fisher Scientific Inc., IL, USA) in the initial homogenate. Specific activity was calculated as nmol of aspartate produced per mg of protein in 1 min (nmol/min/mg protein).

Gas Chromatography–Mass Spectrometry

For measurement of NAA levels, snap-frozen tissue was homogenized in RCP buffer (250 mM saccharose, 50 mH KCl, 5 mM $MgCl_2$, 50 mM Tris, pH 7.4). After centrifugation, the supernatant was kept at −80 °C until further processing. Urine was collected by keeping the mice on metabolic cages

for 4 h per day, and urine samples were kept at −20 °C until further use.

A volume corresponding to 1 μmol creatinine for urine or 250 μl of brain homogenates was used for liquid–liquid extraction. As internal standard, 100 μl of 2,3,3-d3-*N*-acetylaspartic acid (0.1 mM; CDN Isotopes, Canada) was added to each sample. Samples were acidified with 300 mL of 5 M HCl and after addition of solid sodium chloride extracted twice with 5 mL ethyl acetate each time. The combined ethyl acetate fractions were dried over sodium sulfate and then evaporated to dryness at 40 °C under a stream of nitrogen. Samples were then derivatized with 200 μl 3 M butanolic HCl for 30 min at 70 °C. For gas chromatography–mass spectrometry (GC/MS) analysis, the quadrupole mass spectrometer MSD 5972A (Agilent, Santa Rosa, CA, USA) was run in the selective ion-monitoring mode with electron impact ionization. Gas chromatographic separation was achieved on a capillary column (DB-5MS, 30 m× 0.25 mm; film thickness 0.25; J&W Scientific, Folsom, CA, USA) using helium as a carrier gas. A volume of 1 mL of the derivatized sample was injected in splitless mode. GC temperature parameters were 60 °C for 1 min, ramp 50 °C/min to 150 °C, ramp 4 °C/min to 259 °C, and hold for 2 min at 300 °C. Injector temperature was set to 280 °C and interface temperature to 290 °C. Fragment ions for quantification of NAA were *m/z* 186 and *m/z* 189 for denatured NAA. A dwell time of 50 ms was applied.

Proton Magnetic Resonance Spectroscopy (1H-MRS)

All NMR measurements were performed on a 7-Tesla animal scanner (Biospec 70/20 USR, Bruker Biospin, Ettlingen, Germany) equipped with a B_0 gradient system BGA-12S (maximum gradient strength 440 mT/m, rise time 130 μs). While radiofrequency (RF) excitation was performed by a linearly polarized RF resonator (72 mm inner diameter), a four-channel surface coil optimized for rat brain measurements was used for signal reception. The animals were anaesthetized with 0.8–3.0 % isofluorane and oxygen and placed prone in an adjusted animal holder. The MR protocol started with scout images to adjust the position in the magnet and with respect to the RF reception coil. Images from the three orthogonal slices through the magnet center were acquired using a FLASH sequence (Haase et al., 1985) (repetition time TR=100 ms, echo time TE=3 ms, FOV=32 mm × 32 mm, 1.5 mm slice thickness). Subsequently, high-resolution multislice MR imaging was performed using a RARE sequence with the following parameters: FOV 24 × 24 mm^2, 21 slices (0.75 mm thickness, no gap), eight echoes, effective TE 56 ms, 256 × 192 image matrix, TR 5.0 s, two averages, total measurement time 4 min). For single voxel MR spectroscopy, a double spin echo PRESS sequence (Bottomley, 1987) was used (TR 2.5 s, TE 20 ms, 128 averages, spectral width 4,006 Hz). Voxel position and size (typically 12–18 μL) were chosen at the level of the midline of the white matter tract corpus callosum (CC).

The B_0 field homogeneity within the voxel was optimized using the "MAPSHIM" routine based on B_0 field mapping followed by manual optimization of shim coil currents, resulting in a typical line-width of the water signal of about 10–18 Hz. The dominant water signal was suppressed by three consecutive chemical shift selective saturation pulses (CHESS) (Haase et al., 1985). Data processing comprised exponential apodization corresponding to a line broadening by 3.7 Hz, zero filling to 16 K, Fourier transformation, and phase correction.

Statistical Analysis

Two independent experiments were performed with at least four animals per experimental group. For proton magnetic resonance spectroscopy (1H-MRS), two animals were included per independent experiment. Statistical analyses were performed using absolute data. Experimental groups consisted of at least three mice each. Differences between groups were tested by analysis of variance (one-way ANOVA) followed by post hoc testing using Dunnett's Multiple Comparison Test using GraphPad Prism 5 software (GraphPad Software Inc., CA, USA), if not stated otherwise. All data are given as arithmetic means±SEM. *P*-values of the different analyses with $p<0.05$ were considered to be statistically significant (*=$p\leq0.05$; **=$p\leq0.01$; ***=$p\leq0.001$ compared to controls).

Results

Oligodendrocyte Loss Occurs Early in the Cuprizone Model

It has been demonstrated that oligodendrocyte death starts early after initiation of the cuprizone diet (Buschmann et al., 2012; Hesse et al., 2010). Oligodendrocyte death is cell type specific (i.e. only oligodendrocytes) and results from apoptotic processes (i.e. expression of active caspase-3) (Goldberg et al., 2013). Characteristic for NAWM is a significant decrease in the NAA concentration (De Stefano et al., 1999; Sarchielli et al., 1999), reduction in axonal density (Evangelou et al., 2000), as well as astro- and microgliosis (Graumann et al., 2003) with no or only minor alterations in myelin appearance. In a first set of experiments, we aimed to analyze to what extent brains of short-term cuprizone-exposed animals display characteristic features of NAWM in MS patients. To this end, animals were fed cuprizone for up to 1 week, and the white matter tract corpus callosum (CC) was processed for (immuno-) histochemistry. Numerous apoptotic

oligodendrocytes with condensed and/or fragmented nuclei were seen as early as 2 days after initiation of cuprizone intoxication (arrow in Fig. 1a). Such cells were absent in control mice (not shown). In parallel, we found a marked decrease in the number of APC-expressing mature oligodendrocytes (Fig. 1a, b). Comparably, we detected a significant decrease in the number of OLIG2-expressing cells (data not shown) which is another marker protein for oligodendrocytes. Histochemical evaluation of myelination using myelin-specific stainings such as LFB/PAS revealed no demyelination at the histological level (Fig. 1a). To study the relationship between oligodendrocyte stress and early microglia activation, the number of microglia cells was quantified in histological sections using antibodies directed against the microglia/macrophage marker protein IBA1. Microglia cell numbers gradually increased with time during cuprizone treatment (Fig. 1a, c). After 1 week, the number of IBA1+ cells was around six times higher compared to controls. Besides microglia hyperplasia, significant microglia hypertrophy was detected after 1 week (Fig. 1d). The number of GFAP-expressing astrocytes was not altered during the course of the study (Fig. 1a, e). However, real-time PCR analysis and western blotting revealed early activation of astrocytes in this model (Fig. 1f). We furthermore processed the midline of the CC for subsequent analysis at the ultrastructural level. This method revealed signs of dying back oligodendrogliopathy with a splitting of the inner myelin lamella (Fig. 2, arrow) in the CC of cuprizone-exposed mice. Such alterations were absent in control mice. In summary, short-term cuprizone treatment results in early oligodendrocyte stress with concomitant pronounced microglial and moderate astrocyte activation in the absence of overt demyelination.

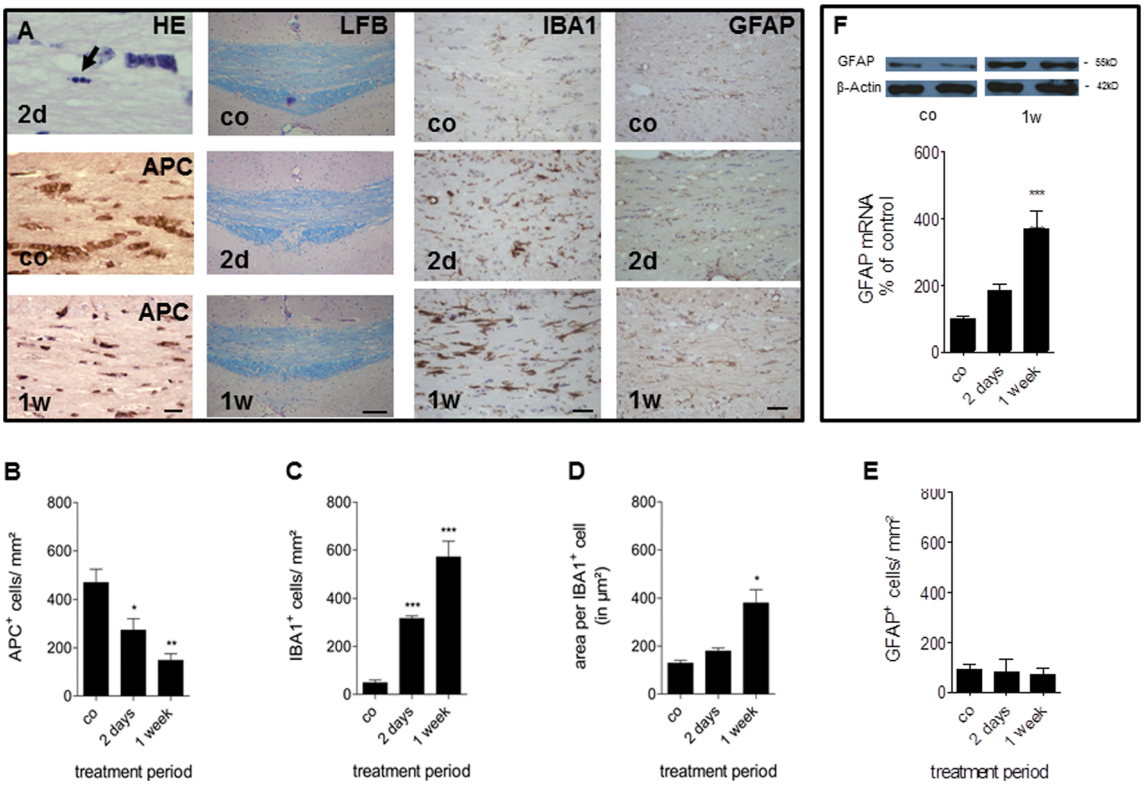

Fig. 1 Characterization of early oligodendrocyte stress in cuprizone-treated mice. **a** *First row, upper part* HE-stained section of the midline of the corpus callosum (*CC*) 2 days (*2d*) after initiation of the cuprizone diet. Note the apoptotic oligodendrocytes (see *arrow*). **a** *First row, lower part* Anti-APC stained sections of the midline of CC in control and mice treated with cuprizone for 1 week (*1w*). **b** Quantification of APC^+ oligodendrocytes in the midline of the CC of control (*co*) and 2 days and 1 week cuprizone-treated mice. Note the lower numbers of APC^+ cells after 2 days and 1 week compared to control mice. **a** *Second row* myelin integrity, determined by LFB/PAS histochemical stains in the CC of control and 2 days and 1 week cuprizone-treated mice. No gross abnormality in myelin was observed on the histological level. **a** *Third row* immunohistochemistry with antibodies directed against the microglial protein IBA1. Note the overt microgliosis in the midline of the CC in mice treated with cuprizone for 1 week. **c** Quantification of $IBA1^+$ cells within the CC revealed significant increase of microglia cell numbers after 2 days and 1 week cuprizone treatment compared to controls. **d** Morphometric quantification of microglia cell area within the CC demonstrates a significant hypertrophy of $IBA1^+$ cells (co 129±11.5, n=3; 2 days 179.1±12.62, n=4; 1 week 379.8±55.12, n=4). **a** *Fourth row* Immunohistochemistry with antibodies against the astrocytic protein GFAP was performed with control, 2 days and 1 week cuprizone treated mice. **e** No increase in astrocyte numbers was evident at day 2 or week 1 compared to controls. **f** GFAP protein levels were detected by western blotting (*upper part*), whereas GFAP mRNA levels were detected by rt-PCR (*lower part*). Note the increased GFAP expression indicating early astrocyte activation. *Scale bars* 10 µm in rows 1, 3, and 4 and 200 µm in row 2

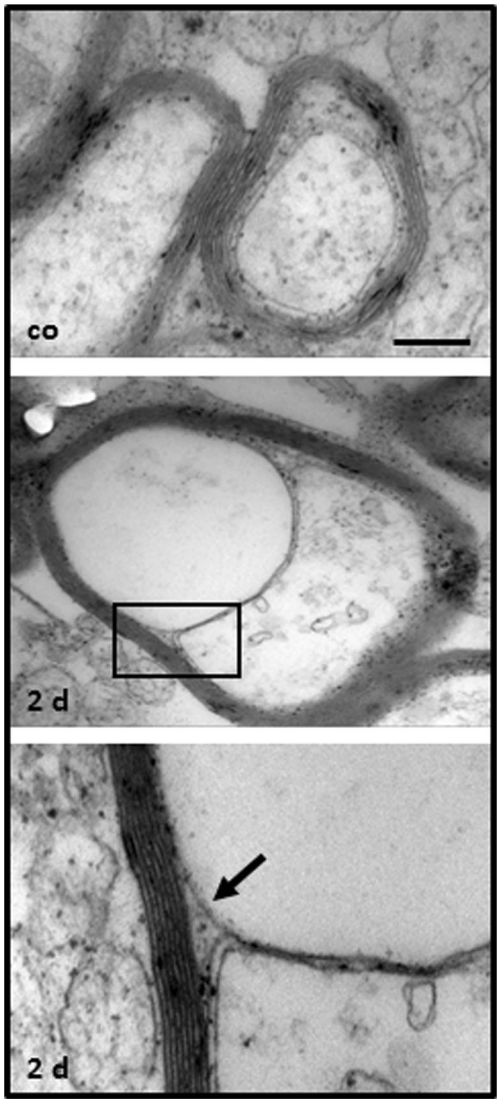

Fig. 2 Characterization of early ultrastructural changes. Electron microscopy of the midline of the CC was performed in control and 2 days cuprizone-treated animals. Note the splitting of innermost myelin lamella (*arrow*). *Scale bar* 1 μm

Early Reduction of Oligodendrocyte-Derived mRNA in the Cuprizone Model

In a next set of experiments, we aimed to identify factors that are linked to oligodendrocyte cell death in the cuprizone model. Total mRNA samples from the CC of mice fed with cuprizone for 2 days were analyzed using Affymetrix GeneChip® arrays. We have chosen this particular time point to reveal changes during initial oligodendrocyte apoptosis. From the genes included in the array, 759 were significantly up-regulated, whereas the expression of 413 was significantly reduced compared to controls. The top 150 genes which displayed the most pronounced down-regulation are given in Table 2. In line with the finding of an early oligodendrocyte dysfunction, many of the down-regulated genes are typically expressed by oligodendrocytes such as fatty acid 2-hydroxylase [Fa2h; 4.48-fold down-regulated, (Eckhardt et al., 2005)], UDP galactosyltransferase 8A [Ugt8a: 3.5-fold down-regulated, (Saadat et al., 2010)], myelin-associated glycoprotein [MAG; 2.99-fold down-regulated (Lax et al., 2012)], as well as proteolipid protein (myelin)-1 [Plp1; 1.72-fold down-regulated] and myelin basic protein [Mbp; 1.53-fold down-regulated (Hartman et al., 1982)]. Other genes which displayed a significant reduction of mRNA levels after 2 days of cuprizone exposure are not typically expressed by oligodendrocytes such as phosphatidylinositol glycan anchor biosynthesis, class Z [Pigz; 2.86-fold down-regulated], and ninjurin 2 [Ninj2; 2.59-fold down-regulated].

Reduced ASPA Gene Expression and Activity due to Cuprizone Treatment Does Not Result in Accumulation of NAA in the Brain

One of the genes found to be significantly lower expressed in the CC of cuprizone-exposed animals is ASPA (1.54-fold down-regulated). First, we verified these gene array findings in a separate set of experiments using rt RT-PCR from combined cortical and CC samples. As shown in Fig. 3a, a dramatic reduction in ASPA mRNA levels was evident after 2 days of cuprizone exposure and remained at these low levels until the end of the follow-up period (i.e. 7 days of cuprizone exposure). Due to the pronounced and early down-regulation of ASPA expression, we investigated in a next set of experiments whether reduced expression levels are paralleled by reduced ASPA enzymatic activity. As shown in Fig. 3b, ASPA activity was significantly diminished after 2 days of cuprizone exposure, indicating that the reduction of ASPA mRNA expression is paralleled by a reduction of ASPA activity—although to a lower extent.

Since NAA is catabolized by the enzyme ASPA (Goldstein, 1959), lower ASPA mRNA expression together with decreased enzymatic activity might result in an increase of NAA tissue levels. To test this hypothesis, we first determined NAA levels in dissected brain samples using GC/MS. As shown in Fig. 3c, NAA levels in brain tissues were not increased after 2 or 7 days of cuprizone exposure. As a positive control, we included corresponding brain tissues from $Aspa^{nur7/nur7}$ mice which virtually lack ASPA activity due to a nonsense mutation (Traka et al., 2008). As expected, increased NAA levels were found in these animals, indicating that the applied assay is sensitive enough to detect even small changes in NAA brain tissue levels. ASPA deficiency in CD patients is paralleled by increased NAA levels in the urine (Matalon et al., 1995). We, therefore, decided to determine NAA levels in the urine of cuprizone-exposed animals. One-way ANOVA, followed by Dunnett's multiple comparison test, revealed that NAA levels in urine samples were significantly increased at day 3 but at all other time points remained stable (Fig. 3d).

Table 2 Genes down-regulated (top 150) after 2 days of cuprizone exposure, as determined by gene array analyses of corpus callosum isolated RNA

	Gene symbol	logFC (2d/co)	Control	Control	Control	2 days	2 days	2 days
1	Mog	−2.57083	12.69443	12.40246	12.37857	9.52852	10.24525	9.98921
2	Ppp1r14a	−2.41357	11.01516	10.58480	10.57721	8.06229	8.68874	8.18544
3	Fa2h	−2.16236	11.76886	11.64332	11.65459	9.46284	9.69121	9.42563
4	Tmem63a	−1.95328	11.27661	11.03273	11.02471	8.98906	9.41747	9.06768
5	Klk6	−1.87317	10.00020	9.77303	9.76959	8.01490	8.17799	7.73041
6	Efhd1	−1.84169	11.41102	11.19088	11.18128	9.21122	9.64088	9.40603
7	Padi2	−1.83811	10.39489	10.14412	10.12684	8.34967	8.57704	8.22482
8	S1pr5	−1.69176	10.64079	10.35519	10.43078	8.44822	9.21629	8.68698
9	Ugt8a	−1.60967	12.12267	11.60536	11.63993	10.16828	10.28788	10.08278
10	Mag	−1.58034	12.97550	12.55970	12.60471	10.87969	11.40672	11.11249
11	Mal	−1.54983	12.34765	12.08535	11.99826	10.31333	10.90821	10.56023
12	Pigz	−1.51341	10.38806	10.39789	10.32761	8.67659	8.96556	8.93117
13	Gsn	−1.47107	10.25219	9.89861	9.81890	8.34245	8.80183	8.41219
14	Gamt	−1.45280	10.82841	10.61384	10.70808	9.22120	9.40950	9.16123
15	Atpgd1	−1.42144	9.72076	9.67504	9.66827	8.28732	8.30030	8.21211
16	Ninj2	−1.37349	9.76154	9.26909	9.43712	8.14120	8.01991	8.18618
17	Thbs4	−1.29420	10.42153	10.19728	10.25775	8.86291	9.30264	8.82842
18	Ttyh2	−1.26169	11.98304	11.72548	11.75773	10.46583	10.70638	10.50898
19	Cpm	−1.20389	9.46971	9.22710	9.44786	8.23692	7.96742	8.32866
20	Gjc2	−1.18675	9.20063	9.04738	8.97474	7.73692	8.17763	7.74795
21	Tspan2	−1.18651	12.27503	11.92327	11.91764	10.61167	11.14744	10.79731
22	Nipal4	−1.18304	9.63595	9.33291	9.59186	8.18243	8.58206	8.24710
23	Cmtm5	−1.15615	12.73921	12.50702	12.50263	11.20787	11.70475	11.36778
24	Tmem98	−1.15499	9.34229	8.95036	9.00276	7.63425	8.49324	7.70296
25	Plxnb3	−1.14033	10.41618	10.17409	10.20106	9.07525	9.30893	8.98617
26	Pstpip2	−1.11350	9.35303	9.59327	9.62650	8.42389	8.32632	8.48208
27	Slc15a2	−1.10524	8.49914	8.94095	9.08821	7.96962	7.54333	7.69962
28	Apln	−1.09432	9.66339	9.69864	9.69334	8.49377	8.83054	8.44810
29	Ptgds	−1.04061	12.09151	12.80458	12.82760	11.15549	11.60651	11.83986
30	Adssl1	−1.03114	10.03292	9.83201	9.76072	8.59275	8.89143	9.04805
31	Gstm7	−1.02994	11.00841	10.94429	11.00452	9.80306	10.00989	10.05444
32	Apod	−1.02919	13.11688	13.03583	13.12024	11.83271	12.17792	12.17476
33	Lrrn1	−1.00763	11.84220	11.61721	11. .66054	10.68758	10.59275	10.81674
34	Pllp	−1.00628	10.84655	10.63908	10.52812	9.57265	9.85998	9.56229
35	Cntn2	−0.99363	11.00896	10.90971	10.99222	9.77278	10.08686	10.07036
36	Fah	−0.97571	10.12372	10.12247	10.12656	9.13529	9.05635	9.25399
37	Serpind1	−0.96358	8.52980	8.59862	8.81953	7.67219	7.80177	7.58324
38	Agt	−0.96122	9.66770	9.87672	9.93436	8.57615	8.72520	9.29378
39	Anln	−0.94815	10.51199	10.33616	10.38091	9.51172	9.50178	9.37112
40	Cryab	−0.94151	12.60882	12.49488	12.50441	11.59849	11.64324	11.54185
41	Mboat1	−0.93107	8.68738	8.61113	8.63237	7.70176	7.74944	7.68648
42	Kndc1	−0.92585	10.71936	10.84551	10.86627	9.67829	9.85726	10.11805
43	Lrp4	−0.91425	9.89998	9.69335	9.70865	8.68058	9.00756	8.87108
44	Slc13a3	−0.91376	9.33879	9.89617	9.79589	8.63301	8.70678	8.94979
45	Nmral1	−0.89399	9.10009	8.81173	8.80789	7.79955	8.11632	8.12186
46	Fzd2	−0.88215	8.85016	8.82758	8.99068	7.84284	8.24435	7.93478
47	Paqr6	−0.87684	9.02861	9.18814	9.33014	8.12287	8.50607	8.28744
48	Gja1	−0.86371	11.56708	11.46566	11.48062	10.68934	10.61727	10.61563
49	Scd1	−0.85586	12.26702	12.31691	12.37030	11.49321	11.47720	11.41623

Table 2 (continued)

	Gene symbol	logFC (2d/co)	Control	Control	Control	2 days	2 days	2 days
50	Fam57a	−0.85138	10.77477	10.71190	10.73429	9.82877	9.88994	9.94812
51	Prrg1	−0.85101	9.06621	8.90013	9.11193	8.14657	8.09500	8.28368
52	Ascl1	−0.83101	10.07425	10.11798	10.14606	9.30879	9.32056	9.21592
53	Hhatl	−0.82514	8.51850	8.58109	8.47540	7.59951	7.54576	7.95431
54	Cyp2j12	−0.81765	9.11923	8.54647	8.54968	7.61369	8.11339	8.03536
55	Aifl1	−0.81519	9.43664	9.09803	9.04150	8.35942	8.48029	8.29090
56	Tubb4	−0.80909	13.41520	13.46963	13.56580	12.71361	12.51718	12.79257
57	Mobkl2b	−0.80654	9.22206	9.15073	9.37303	8.40824	8.66963	8.24833
58	Entpd2	−0.79882	8.55401	8.37471	8.63243	7.68746	7.85734	7.61990
59	2310022B05Rik	−0.79857	10.21875	10.12149	10.16128	9.27783	9. .43732	9.39065
60	Adamts4	−0.79685	10.31657	9.91218	9.90963	9.04048	9.52743	9.17992
61	5031410I06Rik	−0.79652	8.56352	8.37027	8.50204	7.71923	7.67601	7.65101
62	Lpar1	−0.78477	10.59951	10.36908	10.26805	9.52670	9.82809	9.52755
63	Gm410	−0.78461	9.01399	8.41155	8.72844	7.95546	8.03947	7.80522
64	Nfe2l3	−0.78441	8.48454	8.42061	8.43916	7.72888	7.68086	7.58134
65	Chn2	−0.78263	11.48475	11.45459	11.49900	10.74247	10.65121	10.69678
66	Plp1	−0.78212	14.23354	14.09720	14.16719	13.18427	13.59895	13.36835
67	Folh1	−0.78168	9.28562	9.28355	9.40070	8.54740	8.47007	8.60737
68	Il18	−0.77514	9.37791	9.42040	9.39079	8.68908	8.51336	8.66124
69	2600010E01Rik	−0.77510	9.02266	8.64121	8.63780	7.96599	8.14459	7.86580
70	Cldn10	−0.77422	10.69277	10.77098	10.84848	9.86686	9.99490	10.12781
71	Ebp	−0.77285	10.30179	10.18514	10.32842	9.45630	9.60778	9.43272
72	Sass6	−0.76974	8.81375	9.03100	8.97784	8.24480	8.11696	8.15161
73	Pde8a	−0.75877	10.08214	9.77003	9.87733	9.16895	9.14656	9.13769
74	Cldn11	−0.75032	12.83821	12.64254	12.66618	11.86216	12.19632	11.83749
75	Tppp3	−0.74544	11.07670	10.94477	10.92118	10.21105	10.26185	10.23342
76	Trf	−0.74251	12.84157	12.62340	12.57981	11.72912	12.20676	11.88138
77	Phldb1	−0.74250	10.70920	10.38548	10.32317	9.65101	9.86330	9.67605
78	Hapln2	−0.74074	10.15164	9.98807	9.99166	9.28746	9.35024	9.27145
79	Daam2	−0.73566	10.35600	10.33224	10.34605	9.64283	9.72671	9.45778
80	Mtap7	−0.72756	10.86546	10.76965	10.75673	10.09922	10.08630	10.02365
81	Acta2	−0.71167	9.65094	9.96681	9.92146	9.26227	9.13915	9.00278
82	Efnb3	−0.69539	11.03648	10.76583	10.76485	10.11826	10.31434	10.04840
83	Pik3c2b	−0. .69107	10.70676	10.67036	10.58504	10.03507	10.07427	9.77962
84	Galnt6	−0.68668	8.67170	8.44468	8.38004	7.56932	8.11275	7.75432
85	Rasgrp3	−0.68482	10.16018	9.97439	10.04824	9.53830	9.32411	9.26595
86	Sgk1	−0.68463	10.77349	11.03677	11.08494	9.99461	10.51345	10.33326
87	Pdlim1	−0.68211	9.08784	9.35744	9.30297	8.41961	8.32454	8.95777
88	Bgn	−0.68210	9.59658	10.12320	10.09051	9.29913	9.24155	9.22330
89	Sema4d	−0.67735	10.20288	10.10649	10.11564	9.36920	9.59113	9.43263
90	Adamtsl4	−0.67461	8.87595	8.70974	8.71359	8.13853	8.07922	8.05771
91	Abca2	−0.66923	11.76779	11.69554	11.68216	10.97561	11.15348	11.00870
92	Aqp4	−0.66640	10.74125	10.58899	10.56515	9.89680	10.07582	9.92357
93	Scrg1	−0.66587	10.63430	10.71588	10.83225	10.16737	9.88327	10.13417
94	Rnf122	−0.66156	10.16426	9.82965	9.75612	9.10368	9.52121	9.14046
95	Tmem195	−0.66140	8.38803	8.32856	8. .57710	8.04396	7.52326	7.74228
96	Siglech	−0.66132	9.22138	9.16059	9.17955	8.65571	8.33707	8.58478
97	Btd	−0.66080	8.24655	8.30212	8.57000	7.55775	7.87976	7.69875
98	Zdhhc9	−0.65792	11.40837	11.45483	11.46623	10.80040	10.81690	10.73837

Table 2 (continued)

	Gene symbol	logFC (2d/co)	Control	Control	Control	2 days	2 days	2 days
99	Pld1	−0.63669	9.15128	9.27713	9.22400	8.51417	8.69542	8.53273
100	ENSMUSG00000073675	−0.63626	8.79165	8.52979	8.72193	7.92792	8.05919	8.14750
101	Gdpd2	−0.63484	8.40245	8.49278	8.49471	7.78618	7.86240	7.83684
102	Spsb1	−0.63388	10.19514	10.33066	10.39419	9.70082	9.56896	9.74857
103	Plekhg3	−0.62249	9.42251	9.15660	9.16245	8.62791	8.73931	8.50686
104	Cercam	−0.62186	8.46560	8.28045	8.30641	7.62991	7.88504	7.67193
105	Map6d1	−0.62059	11.29072	11.10146	11.17606	10.54080	10.62172	10.54396
106	Aspa	−0.61870	10.56583	10.10943	10.21034	9.66718	9.69910	9.66322
107	Tmeff2	−0.61694	11.99861	11.74187	11.75827	11.07688	11.31555	11.25549
108	Mbp	−0.61684	13.11684	12.99302	13.01577	12.39967	12.46463	12.41082
109	Psd2	−0.61369	9.88137	10.02793	9.96964	9.23936	9.53801	9.26051
110	Ppap2c	−0.61240	9.89196	9.58004	9.47825	8.89071	9.30082	8.92150
111	ENSMUSG00000075555	−0.60986	8.54849	8.12807	8.19622	7.81600	7.64323	7.58398
112	Car2	−0.60403	12.28682	11.91066	11.91896	11.29951	11.61205	11.39278
113	M6prbp1	−0.60299	9.22650	8.90722	8.92488	8.21672	8.60165	8.43125
114	Kctd4	−0.60098	9.27673	9.40956	9.49982	8.90829	8.67957	8.79532
115	Cyp27a1	−0.60029	9.02834	8.76274	8.73737	8.14964	8.27303	8.30491
116	Pctk3	−0.59742	9.96362	10.04225	9.95389	9.20781	9.45198	9.50770
117	Papss2	−0.59636	9.33719	9.52484	9.59524	8.89640	8.95182	8.81996
118	Slc44a1	−0.59220	11.76010	11.52031	11.53722	10.88136	11.17134	10.98833
119	Scara3	−0.59217	9.36485	9.34065	9.30147	8.61252	8.78479	8.83317
120	AI464131	−0.59119	8.91727	8.95790	9.03337	8.23550	8.54722	8.35225
121	AY512949	−0.58761	9.48180	9.95427	9.94807	9.35909	9.00678	9.25544
122	Trim13	−0.58650	10.15191	9.77860	9.88561	9.50415	9.14068	9.41180
123	Ermn	−0.58510	11.74725	11.32020	11.42077	10.94526	10.95881	10.82886
124	Lama2	−0.58507	8.62347	8.59084	8.70670	8.06109	8.05948	8.04522
125	Itgb4	−0.58380	8.85708	8.85216	8.83086	8.19108	8.36426	8.23336
126	Hist1h2ak	−0.58338	10.54357	10.26343	10.31258	9.84148	9.80641	9.72157
127	6330503K22Rik	−0.58004	10.48622	10.22967	10.26624	9.64347	9.83386	9.76469
128	Lass2	−0.57791	12.05402	11.66872	11.71651	11.11164	11.34097	11.25291
129	Adi1	−0.57534	10.54359	10.45333	10.44799	9.91330	9.89763	9.90795
130	Rhog	−0.57340	10.96783	10.65983	10.75641	10.09721	10.34483	10.22182
131	Speer8−ps1	−0.57058	8.43078	8.42335	8.40542	8.01432	7.88605	7.64745
132	Tmem163	−0.56935	11.21063	11.29670	11.32953	10.80589	10.65856	10.66435
133	Myo1d	−0.56761	10.25950	10.21574	10.26676	9.62331	9.88936	9.52651
134	Dusp15	−0.56701	9.30090	9.37024	9.50319	8.79324	8.78423	8.89584
135	Acy3	−0.56690	8.46955	8.44379	8.50049	8.01476	7.85586	7.84249
136	Mfge8	−0.56682	11.41611	11.44622	11.37299	10.85850	10.94126	10.73509
137	Sept4	−0.56625	11.54243	10.96664	11.01498	10.57036	10.59459	10.66036
138	Rftn2	−0.56555	8.99058	8.93199	8.99997	8.37934	8.45250	8.39406
139	Plod1	−0.56257	10.06016	9.89809	9.89043	9.16046	9.53661	9.46391
140	Cyth1	−0.55950	10.30165	10.27593	10.30255	9.73122	9.67754	9.79286
141	Dio2	−0.55908	9.65488	9.70899	9.78503	9.15586	9.20795	9.10787
142	Phkg1	−0.55678	8.49928	8.31048	8.35576	7.91645	7.70976	7.86896
143	4933428G20Rik	−0.55461	10.31956	10.14286	10.18440	9.51503	9.77910	9.68886
144	Alpl	−0.55323	8.30681	8.48508	8.52584	7.85026	8.00198	7.80580
145	Gal3st1	−0.55308	10.37383	8.64641	8.40484	8.25582	7.80242	7.92284
146	Fmo1	−0.55252	10.35957	9.15556	9.02929	9.14820	8.51613	8.47424
147	A230069A22Rik	−0.55211	10.51920	11.40031	11.05096	11.13266	10.45583	10.63126

Table 2 (continued)

	Gene symbol	logFC (2d/co)	Control	Control	Control	2 days	2 days	2 days
148	Prdx6	−0.54643	10.35942	11.32591	11.08222	11.13466	10.49613	10.75971
149	Gpr62	−0.53593	9.032417	8.774814	8.764187	8.267071	8.35828	8.338271
150	Ccdc74a	−0.53541	9.199626	9.248755	9.465782	8.754852	8.680931	8.872149

Finally, we estimated NAA levels in the living animal by using 1H-MRS (Dreher et al., 2001). In line with our findings from the previous experiments, no obvious difference exists in the NAA signal intensity between control and cuprizone-exposed animals (see Fig. 4).

Early Axonal Damage Is Not a Characteristic Feature in the Cuprizone Model

So far, we were able to demonstrate that a reduction of ASPA mRNA expression and activity is not paralleled by the accumulation of NAA in the brain of cuprizone-intoxicated animals. Since NAA is almost exclusively located in neurons and their processes in the brain (Moffett et al., 1991; Simmons et al., 1991), we deemed it mandatory to rule out that neurodegeneration occurs in the early stage of cuprizone intoxication. To test for this possibility, we performed IHC against the synaptic protein APP. The accumulation of APP which is transported along axons in an anterograde fashion indicates a putative dysfunction of the axonal transport mechanisms and precedes axon fragmentation (Ferguson et al., 1997; Schirmer et al., 2013). Anti-APP IHC is therefore a valid marker to visualize acute axonal damage. As demonstrated in Fig. 5, APP^+ spheroids are not seen in control animals but are readily detectable after 5 weeks of cuprizone exposure (arrows in Fig. 5). Notably, no significant increase in APP^+ spheroids is evident after 1 week of cuprizone treatment, indicating that neurodegeneration has not yet started at this early time point.

Discussion

Numerous studies highlight the importance of NAA 1H-MRS for the evaluation and follow-up of MS patients. Results using this method suggest that (1) axonal damage occurs early

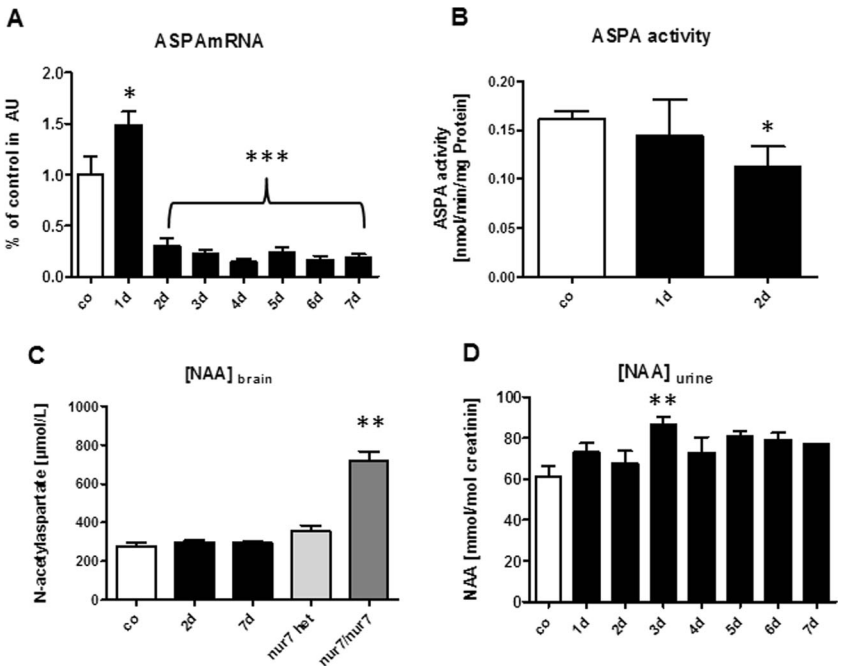

Fig. 3 Changes in *N*-acetylaspartate metabolism. **a** Aspartoacylase (*ASPA*) expression during the first week of cuprizone intoxication. Note the early and pronounced reduction in ASPA expression levels. **b** ASPA activity determined by an enzymatic assay. Note the significant reduction of ASPA activity after 2 days of cuprizone exposure (tested by unpaired *t*-test). **c** *N*-Acetylaspartate (*NAA*) levels in brain tissue after cuprizone exposure, determined by gas chromatography–mass spectrometry. Note the stable NAA levels in brain tissue treated up to 1 week with cuprizone. Further note the increased NAA levels in tissues isolated from animals harbouring an ASPA mutation (nur7/nur7 mutation). **d** NAA levels in urine after cuprizone exposure, as determined by GC/MS

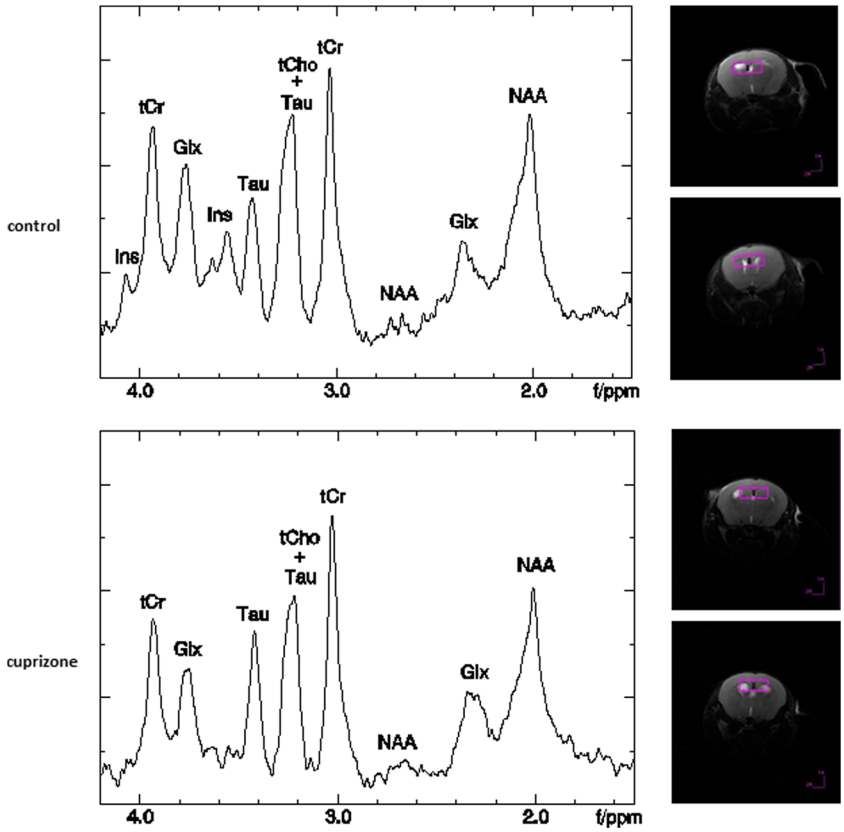

Fig. 4 Proton magnetic resonance spectroscopy of cuprizone-treated mice. Representative in vivo proton spectra from a control animal and a cuprizone-treated mouse for 1 week is shown on the *left side*. The *right side* illustrates the region of interest, highlighted by a *red box* (i.e. midline of the corpus callosum). *Ins* myo-inositol, *tCr* total creatinine, *Glx* glutamine+glutamate, *Tau* taurine, *tCho* choline-containing compounds, *NAA N*-acetylaspartate

during disease course (Wattjes et al., 2007; Wattjes et al., 2008), (2) glatiramer acetate is neuroprotective in RRMS (Khan et al., 2005), (3) Wallerian degeneration is present early in the disease, and (4) neurodegeneration relates to selective attention impairment in early-stage RRMS (Gadea et al., 2004). Furthermore, other studies reported reduced NAA levels in the NAWM of MS patients, mirroring neuronal/axonal damage (Gustafsson et al., 2007; Wattjes et al., 2008). However, since results of some reports came up with conflicting results regarding reductions of NAA levels in the NAWM of MS brains (Fernando et al., 2004; Vrenken et al., 2005), we addressed in this study whether oligodendrocyte pathology might interfere with NAA levels in the NAWM of MS patients using the cuprizone animal model.

We were able to demonstrate by various techniques that dysfunction of oligodendrocytes is an early and significant event in this toxic animal model. Our observation of early apoptosis of oligodendrocytes is in line with reports from other groups. Hesse and colleagues were able to show that oligodendroglial cell death and down-regulation of myelin-related mRNA transcripts starts days after initiation of the cuprizone diet and weeks before demyelination is obvious (Hesse et al., 2010). Furthermore, they were able to demonstrate that in the early but not in the later stages, dying oligodendrocytes express activated caspase 3, suggesting a switch from classical apoptotic pathways to caspase 3-independent mechanisms during the course of the cuprizone diet. Recent studies from our group confirmed these findings

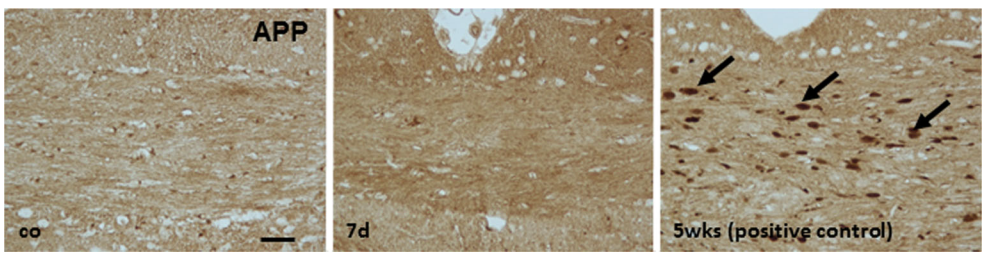

Fig. 5 Acute axonal damage in cuprizone-treated animals. Acute axonal damage determined by immunohistochemistry against amlyoid precursor protein (*APP*). Note the absence of APP^+ spheroids in control and 1 week cuprizone-treated animals. Further note the intense accumulation of APP^+ spheroids after 5 weeks of cuprizone exposure (*arrows*), verifying the presence of acute axonal damage. *Scale bar* 25 μm

(Buschmann et al., 2012) and further highlighted that oligodendrocyte apoptosis is not restricted to the CC but can be found in various brain regions (Kipp et al., 2011b). In the present study, we furthermore show that sites of periaxonal oligodendrocyte processes are affected, too (see Fig. 2), a phenomenon called "dying-back oligodendrogliopathy" (Lassmann et al., 1997). Similar alterations of oligodendrocytes have been described in brain biopsies from MS plaques (Rodriguez and Scheithauer, 1994) and in demyelinating lesions of Theiler's virus-induced encephalomyelitis (Rodriguez, 1992).

The rational why we favoured the cuprizone model in this study is manifold. First, oligodendrocyte dysfunction follows a predictable time course and occurs at distinct brain regions among the CC and the telencephalic cortex (Acs et al., 2009; Kipp et al., 2009; Skripuletz et al., 2011). Furthermore, peripheral immune cell recruitment is not a cardinal feature in this model (Mildner et al., 2007) and, thus, provides a reductionist tool to study mechanisms operant during brain intrinsic neuroinflammatory events. Another indispensable condition to study the impact of oligodendrocyte NAA metabolism on NAA accumulation is the absence of axonal or neuronal damage at sites of oligodendrocyte injury. If axonal or neuronal damage occurs, NAA levels are expected to decrease and, therefore, the accumulation of NAA due to disturbed oligodendrocyte metabolism might be clouded. As demonstrated in Fig. 5, accumulation of APP^{+} spheroids cannot be detected until week 1, indicating that axonal integrity (i.e. anterograde axonal transport) is not yet disturbed during early cuprizone-induced oligodendrogliopathy.

Some controversy exists regarding the expression of ASPA in the brain. Although ASPA appears to be enriched in oligodendrocytes (Klugmann et al., 2005; Traka et al., 2008; Wang et al., 2007), other brain cell types such as microglia and neurons have been reported to express ASPA (Madhavarao et al., 2004; Moffett et al., 2011). Despite the detected oligodendrogliopathy, our results show constant NAA levels in brain tissue, suggesting that NAA levels are not influenced by oligodendrogliopathy. Therefore, we might assume that neuronal damage in MS patients could be adequately represented by measurement of NAA levels via NAA 1H-MRS. Why NAA levels remain stable despite reductions in ASPA activity remains to be clarified. One possibility is that NAA leaves the brain and is excreted by the urinary tract. Indeed in patients suffering from CD, NAA levels are increased in the urine. In our studies, only a transient increase in NAA urine levels was apparent during the course of cuprizone intoxication. As shown in Fig. 3d, NAA levels rose from ~60 to 90 mmol/mmol creatinine at day 3, but during all other investigated time points, NAA levels remained stable. To our knowledge, no data exist regarding NAA urine levels in MS patients. Thus, we cannot exclude the possibility that NAA is excreted by the urinary tract and, therefore, does not accumulate in the brain of cuprizone-treated animals. Since astrocytes do not express ASPA (Madhavarao et al., 2004), we consider it more likely that other glia cells, such microglia, which are both early in this model (compare Fig. 1), metabolize NAA and, therefore, prevent accumulation of NAA in brain tissue. Indeed expression of ASPA in microglia has been reported (Madhavarao et al., 2004; Moffett et al., 2011), and the local activation of microglia is a well-described feature of early MS lesions (Barnett and Prineas, 2004; Henderson et al., 2009; van der Valk and Amor, 2009). In contrast, ASPA appears not to be expressed by astrocytes (Madhavarao et al., 2004). Nevertheless, it has been suggested that astrocytes play a role in removal of NAA from the extracellular space by its uptake via a specific NAA transporter (Sager et al., 1999). Furthermore, astrocytes do contain high levels of amidohydrolase I activity (Baslow et al., 2001), a broad-spectrum enzyme against peptides and acetylated amino acids that also has low activity against NAA. Therefore, NAA removal from the brain via the sodium-dependent high-affinity dicarboxylate transporter, Slc13a3, at the astrocyte surface, and its hydrolysis by astrocyte amidohydrolase I might be operant (Baslow, 2003).

Results of our genome-wide array analysis underpin the relevance of early oligodendrocyte dysfunction in this model. As early as 2 days after initiation of the cuprizone challenge, the expression of 413 genes was significantly reduced compared to controls. As one would expect, classical myelin-related genes displayed significantly reduced expression levels, among them myelin oligodendrocyte glycoprotein (MOG), myelin-associated glycoprotein (MAG), myelin and lymphocyte protein (MAL), or proteolipid protein 1 (PLP1). This observation is in line with recently published findings which show that, in pathology-free regions of MS-affected brains, genes regulating oligodendrocyte survival are hypermethylated and expressed at lower levels while genes related to proteolytic processing are hypomethylated and expressed at higher levels (Huynh et al., 2014). Thus, changes in genes affecting oligodendrocyte susceptibility to damage are detected in pathology-free areas of MS-affected brains.

However, several genes which displayed a dramatic reduction in mRNA levels have not yet been reported in the literature to be expressed by oligodendrocytes, including Ppp1r14a (also known as C-potentiated myosin phosphatase inhibitor of 17 kDa) which is preferentially expressed in smooth muscle cells (Su et al., 2013) or EF hand domain containing 1 (EFhd1), also known as Swiprosin-2. Interestingly, it has been suggested that Swiprosin-2/EFhd1 modulates apoptosis and differentiation of neuronal and muscle precursor cells, probably through an association with mitochondria. Furthermore, it was emphasized that Swiprosin-2/EFhd1 is part of a cellular response to oxidative stress which could explain its pro-survival activity in neuronal, muscle, and malignant tissues (Dutting et al., 2011). Although the assumption that both

factors, Ppp1r14a and EFhd1, are indeed expressed by oligodendrocytes lacks formal approval, our gene array results come up with putative novel proteins expressed by oligodendrocytes. Further studies, however, have to show the relevance of these factors for oligodendrocyte death and/or myelin repair.

In summary, our novel findings underpin the reliability of NAA quantification as a valid marker for the para-clinical determination of the extent of neurodegeneration, even in situations when oligodendrocytes are lost and therefore are unable to metabolize NAA. Future studies have to reveal whether other enzymes are able to metabolize NAA and an excess of NAA is cleared by other mechanisms rather than enzymatic metabolism.

Acknowledgments We would like to thank Helga Helten, Petra Ibold and Wouter Gerritsen for excellent technical assistance. This study was supported by a grant from ProMyelo - SFZ

References

Acs P, Kipp M, Norkute A, Johann S, Clarner T, Braun A, Berente Z, Komoly S, Beyer C (2009) 17beta-estradiol and progesterone prevent cuprizone provoked demyelination of corpus callosum in male mice. Glia 57:807–814

Acs P, Selak MA, Komoly S, Kalman B (2013) Distribution of oligodendrocyte loss and mitochondrial toxicity in the cuprizone-induced experimental demyelination model. J Neuroimmunol 262:128–131

Barnett MH, Prineas JW (2004) Relapsing and remitting multiple sclerosis: pathology of the newly forming lesion. Ann Neurol 55:458–468

Baslow MH (2003) *N*-acetylaspartate in the vertebrate brain: metabolism and function. Neurochem Res 28:941–953

Baslow MH, Suckow RF, Berg MJ, Marks N, Saito M, Bhakoo KK (2001) Differential expression of carnosine, homocarnosine and *N*-acetyl-L-histidine hydrolytic activities in cultured rat macroglial cells. J Mol Neurosci 17:351–359

Bhakoo KK, Craig TJ, Styles P (2001) Developmental and regional distribution of aspartoacylase in rat brain tissue. J Neurochem 79: 211–220

Bitsch A, Bruhn H, Vougioukas V, Stringaris A, Lassmann H, Frahm J, Bruck W (1999) Inflammatory CNS demyelination: histopathologic correlation with in vivo quantitative proton MR spectroscopy. AJNR Am J Neuroradiol 20:1619–1627

Bjartmar C, Kidd G, Mork S, Rudick R, Trapp BD (2000) Neurological disability correlates with spinal cord axonal loss and reduced *N*-acetyl aspartate in chronic multiple sclerosis patients. Ann Neurol 48:893–901

Bjartmar C, Battistuta J, Terada N, Dupree E, Trapp BD (2002) *N*-Acetylaspartate is an axon-specific marker of mature white matter in vivo: a biochemical and immunohistochemical study on the rat optic nerve. Ann Neurol 51:51–58

Bottomley PA (1987) Spatial localization in NMR spectroscopy in vivo. Ann N Y Acad Sci 508:333–348

Buschmann JP, Berger K, Awad H, Clarner T, Beyer C, Kipp M (2012) Inflammatory response and chemokine expression in the white matter corpus callosum and gray matter cortex region during cuprizone-induced demyelination. J Mol Neurosci 48:66–76

Clarner T, Diederichs F, Berger K, Denecke B, Gan L, van der Valk P, Beyer C, Amor S, Kipp M (2012) Myelin debris regulates inflammatory responses in an experimental demyelination animal model and multiple sclerosis lesions. Glia 60:1468–1480

Clarner, T., Wieczorek, N., Krauspe, B., Jansen, K., Beyer, C., Kipp, M., 2013. Astroglial redistribution of aquaporin 4 during spongy degeneration in a Canavan disease mouse model. J Mol Neurosci

Davie CA, Barker GJ, Webb S, Tofts PS, Thompson AJ, Harding AE, McDonald WI, Miller DH (1995) Persistent functional deficit in multiple sclerosis and autosomal dominant cerebellar ataxia is associated with axon loss. Brain 118(Pt 6):1583–1592

Davie CA, Barker GJ, Thompson AJ, Tofts PS, McDonald WI, Miller DH (1997) 1H magnetic resonance spectroscopy of chronic cerebral white matter lesions and normal appearing white matter in multiple sclerosis. J Neurol Neurosurg Psychiatry 63:736–742

De Stefano N, Narayanan S, Matthews PM, Francis GS, Antel JP, Arnold DL (1999) In vivo evidence for axonal dysfunction remote from focal cerebral demyelination of the type seen in multiple sclerosis. Brain 122(Pt 10):1933–1939

De Stefano N, Narayanan S, Francis GS, Arnaoutelis R, Tartaglia MC, Antel JP, Matthews PM, Arnold DL (2001) Evidence of axonal damage in the early stages of multiple sclerosis and its relevance to disability. Arch Neurol 58:65–70

Dreher W, Busch E, Leibfritz D (2001) Changes in apparent diffusion coefficients of metabolites in rat brain after middle cerebral artery occlusion measured by proton magnetic resonance spectroscopy. Magn Reson Med 45:383–389

Dutting S, Brachs S, Mielenz D (2011) Fraternal twins: Swiprosin-1/EFhd2 and Swiprosin-2/EFhd1, two homologous EF-hand containing calcium binding adaptor proteins with distinct functions. Cell Commun Signal 9:2

Eckhardt M, Yaghootfam A, Fewou SN, Zoller I, Gieselmann V (2005) A mammalian fatty acid hydroxylase responsible for the formation of alpha-hydroxylated galactosylceramide in myelin. Biochem J 388: 245–254

Evangelou N, Esiri MM, Smith S, Palace J, Matthews PM (2000) Quantitative pathological evidence for axonal loss in normal appearing white matter in multiple sclerosis. Ann Neurol 47:391–395

Ferguson B, Matyszak MK, Esiri MM, Perry VH (1997) Axonal damage in acute multiple sclerosis lesions. Brain 120(Pt 3):393–399

Fernando KT, McLean MA, Chard DT, MacManus DG, Dalton CM, Miszkiel KA, Gordon RM, Plant GT, Thompson AJ, Miller DH (2004) Elevated white matter myo-inositol in clinically isolated syndromes suggestive of multiple sclerosis. Brain 127:1361–1369

Gadea M, Martinez-Bisbal MC, Marti-Bonmati L, Espert R, Casanova B, Coret F, Celda B (2004) Spectroscopic axonal damage of the right locus coeruleus relates to selective attention impairment in early stage relapsing–remitting multiple sclerosis. Brain 127:89–98

Goldberg J, Daniel M, van Heuvel Y, Victor M, Beyer C, Clarner T, Kipp M (2013) Short-term cuprizone feeding induces selective amino acid deprivation with concomitant activation of an integrated stress response in oligodendrocytes. Cell Mol Neurobiol 33:1087–1098

Goldstein FB (1959) Biosynthesis of *N*-acetyl-L-aspartic acid. Biochim Biophys Acta 33:583–584

Graumann U, Reynolds R, Steck AJ, Schaeren-Wiemers N (2003) Molecular changes in normal appearing white matter in multiple sclerosis are characteristic of neuroprotective mechanisms against hypoxic insult. Brain Pathol 13:554–573

Gustafsson MC, Dahlqvist O, Jaworski J, Lundberg P, Landtblom AM (2007) Low choline concentrations in normal-appearing white matter of patients with multiple sclerosis and normal MR imaging brain scans. AJNR Am J Neuroradiol 28:1306–1312

Haase A, Frahm J, Hanicke W, Matthaei D (1985) 1H NMR chemical shift selective (CHESS) imaging. Phys Med Biol 30:341–344

Hartman BK, Agrawal HC, Agrawal D, Kalmbach S (1982) Development and maturation of central nervous system myelin: comparison of immunohistochemical localization of proteolipid

protein and basic protein in myelin and oligodendrocytes. Proc Natl Acad Sci U S A 79:4217–4220

Henderson AP, Barnett MH, Parratt JD, Prineas JW (2009) Multiple sclerosis: distribution of inflammatory cells in newly forming lesions. Ann Neurol 66:739–753

Hesse A, Wagner M, Held J, Bruck W, Salinas-Riester G, Hao Z, Waisman A, Kuhlmann T (2010) In toxic demyelination oligodendroglial cell death occurs early and is FAS independent. Neurobiol Dis 37:362–369

Huynh JL, Garg P, Thin TH, Yoo S, Dutta R, Trapp BD, Haroutunian V, Zhu J, Donovan MJ, Sharp AJ, Casaccia P (2014) Epigenome-wide differences in pathology-free regions of multiple sclerosis-affected brains. Nat Neurosci 17:121–130

Irizarry RA, Bolstad BM, Collin F, Cope LM, Hobbs B, Speed TP (2003) Summaries of Affymetrix GeneChip probe level data. Nucleic Acids Res 31:e15

Johann S, Kampmann E, Denecke B, Arnold S, Kipp M, Mey J, Beyer C (2008) Expression of enzymes involved in the prostanoid metabolism by cortical astrocytes after LPS-induced inflammation. J Mol Neurosci 34:177–185

Khan O, Shen Y, Caon C, Bao F, Ching W, Reznar M, Buccheister A, Hu J, Latif Z, Tselis A, Lisak R (2005) Axonal metabolic recovery and potential neuroprotective effect of glatiramer acetate in relapsing–remitting multiple sclerosis. Mult Scler 11:646–651

Kipp M, Norkute A, Johann S, Lorenz L, Braun A, Hieble A, Gingele S, Pott F, Richter J, Beyer C (2008) Brain-region-specific astroglial responses in vitro after LPS exposure. J Mol Neurosci 35:235–243

Kipp M, Clarner T, Dang J, Copray S, Beyer C (2009) The cuprizone animal model: new insights into an old story. Acta Neuropathol 118: 723–736

Kipp M, Gingele S, Pott F, Clarner T, van der Valk P, Denecke B, Gan L, Siffrin V, Zipp F, Dreher W, Baumgartner W, Pfeifenbring S, Godbout R, Amor S, Beyer C (2011a) BLBP-expression in astrocytes during experimental demyelination and in human multiple sclerosis lesions. Brain Behav Immun 25:1554–1568

Kipp M, Norkus A, Krauspe B, Clarner T, Berger K, van der Valk P, Amor S, Beyer C (2011b) The hippocampal fimbria of cuprizone-treated animals as a structure for studying neuroprotection in multiple sclerosis. Inflamm Res 60:723–726

Kirov II, Tal A, Babb JS, Herbert J, Gonen O (2013) Serial proton MR spectroscopy of gray and white matter in relapsing–remitting MS. Neurology 80:39–46

Klugmann M, Leichtlein CB, Symes CW, Serikawa T, Young D, During MJ (2005) Restoration of aspartoacylase activity in CNS neurons does not ameliorate motor deficits and demyelination in a model of Canavan disease. Mol Ther 11:745–753

Lassmann H, Bartsch U, Montag D, Schachner M (1997) Dying-back oligodendrogliopathy: a late sequel of myelin-associated glycoprotein deficiency. Glia 19:104–110

Lax NZ, Campbell GR, Reeve AK, Ohno N, Zambonin J, Blakely EL, Taylor RW, Bonilla E, Tanji K, DiMauro S, Jaros E, Lassmann H, Turnbull DM, Mahad DJ (2012) Loss of myelin-associated glycoprotein in Kearns–Sayre syndrome. Arch Neurol 69:490–499

Lund H, Krakauer M, Skimminge A, Sellebjerg F, Garde E, Siebner HR, Paulson OB, Hesse D, Hanson LG (2013) Blood–brain barrier permeability of normal appearing white matter in relapsing–remitting multiple sclerosis. PLoS One 8:e56375

Madhavarao CN, Hammer JA, Quarles RH, Namboodiri MA (2002) A radiometric assay for aspartoacylase activity in cultured oligodendrocytes. Anal Biochem 308:314–319

Madhavarao CN, Moffett JR, Moore RA, Viola RE, Namboodiri MA, Jacobowitz DM (2004) Immunohistochemical localization of aspartoacylase in the rat central nervous system. J Comp Neurol 472:318–329

Matalon R, Michals K, Kaul R (1995) Canavan disease: from spongy degeneration to molecular analysis. J Pediatr 127:511–517

Mattan NS, Ghiani CA, Lloyd M, Matalon R, Bok D, Casaccia P, de Vellis J (2010) Aspartoacylase deficiency affects early postnatal development of oligodendrocytes and myelination. Neurobiol Dis 40:432–443

Mildner A, Schmidt H, Nitsche M, Merkler D, Hanisch UK, Mack M, Heikenwalder M, Bruck W, Priller J, Prinz M (2007) Microglia in the adult brain arise from Ly-6ChiCCR2+ monocytes only under defined host conditions. Nat Neurosci 10:1544–1553

Mistry N, Abdel-Fahim R, Mougin O, Tench C, Gowland P, Evangelou N (2014) Cortical lesion load correlates with diffuse injury of multiple sclerosis normal appearing white matter. Mult Scler 20: 227–233

Moffett JR, Namboodiri MA, Cangro CB, Neale JH (1991) Immunohistochemical localization of *N*-acetylaspartate in rat brain. Neuroreport 2:131–134

Moffett JR, Ross B, Arun P, Madhavarao CN, Namboodiri AM (2007) *N*-Acetylaspartate in the CNS: from neurodiagnostics to neurobiology. Prog Neurobiol 81:89–131

Moffett JR, Arun P, Ariyannur PS, Garbern JY, Jacobowitz DM, Namboodiri AM (2011) Extensive aspartoacylase expression in the rat central nervous system. Glia 59:1414–1434

Norkute A, Hieble A, Braun A, Johann S, Clarner T, Baumgartner W, Beyer C, Kipp M (2009) Cuprizone treatment induces demyelination and astrocytosis in the mouse hippocampus. J Neurosci Res 87:1343–1355

Pott F, Gingele S, Clarner T, Dang J, Baumgartner W, Beyer C, Kipp M (2009) Cuprizone effect on myelination, astrogliosis and microglia attraction in the mouse basal ganglia. Brain Res 1305: 137–149

Rigotti DJ, Inglese M, Gonen O (2007) Whole-brain *N*-acetylaspartate as a surrogate marker of neuronal damage in diffuse neurologic disorders. AJNR Am J Neuroradiol 28:1843–1849

Rodriguez M (1992) Central nervous system demyelination and remyelination in multiple sclerosis and viral models of disease. J Neuroimmunol 40:255–263

Rodriguez M, Scheithauer B (1994) Ultrastructure of multiple sclerosis. Ultrastruct Pathol 18:3–13

Saadat L, Dupree JL, Kilkus J, Han X, Traka M, Proia RL, Dawson G, Popko B (2010) Absence of oligodendroglial glucosylceramide synthesis does not result in CNS myelin abnormalities or alter the dysmyelinating phenotype of CGT-deficient mice. Glia 58:391–398

Sager TN, Thomsen C, Valsborg JS, Laursen H, Hansen AJ (1999) Astroglia contain a specific transport mechanism for *N*-acetyl-L-aspartate. J Neurochem 73:807–811

Sarchielli P, Presciutti O, Pelliccioli GP, Tarducci R, Gobbi G, Chiarini P, Alberti A, Vicinanza F, Gallai V (1999) Absolute quantification of brain metabolites by proton magnetic resonance spectroscopy in normal-appearing white matter of multiple sclerosis patients. Brain 122(Pt 3):513–521

Schirmer L, Merkler D, Konig FB, Bruck W, Stadelmann C (2013) Neuroaxonal regeneration is more pronounced in early multiple sclerosis than in traumatic brain injury lesions. Brain Pathol 23:2–12

Simmons ML, Frondoza CG, Coyle JT (1991) Immunocytochemical localization of *N*-acetyl-aspartate with monoclonal antibodies. Neuroscience 45:37–45

Skripuletz T, Gudi V, Hackstette D, Stangel M (2011) De- and remyelination in the CNS white and grey matter induced by cuprizone: the old, the new, and the unexpected. Histol Histopathol 26:1585–1597

Stadelmann C (2011) Multiple sclerosis as a neurodegenerative disease: pathology, mechanisms and therapeutic implications. Curr Opin Neurol 24:224–229

Su W, Xie Z, Liu S, Calderon LE, Guo Z, Gong MC (2013) Smooth muscle-selective CPI-17 expression increases vascular smooth

muscle contraction and blood pressure. Am J Physiol Heart Circ Physiol 305:H104–H113

Tallan HH, Moore S, Stein WH (1956) *N*-Acetyl-L-aspartic acid in brain. J Biol Chem 219:257–264

Traka M, Wollmann RL, Cerda SR, Dugas J, Barres BA, Popko B (2008) Nur7 is a nonsense mutation in the mouse aspartoacylase gene that causes spongy degeneration of the CNS. J Neurosci 28:11537–11549

van der Valk P, Amor S (2009) Preactive lesions in multiple sclerosis. Curr Opin Neurol 22:207–213

Vrenken H, Barkhof F, Uitdehaag BM, Castelijns JA, Polman CH, Pouwels PJ (2005) MR spectroscopic evidence for glial increase but not for neuro-axonal damage in MS normal-appearing white matter. Magn Reson Med 53:256–266

Wang J, Matalon R, Bhatia G, Wu G, Li H, Liu T, Lu ZH, Ledeen RW (2007) Bimodal occurrence of aspartoacylase in myelin and cytosol of brain. J Neurochem 101:448–457

Wattjes MP, Harzheim M, Lutterbey GG, Klotz L, Schild HH, Traber F (2007) Axonal damage but no increased glial cell activity in the normal-appearing white matter of patients with clinically isolated syndromes suggestive of multiple sclerosis using high-field magnetic resonance spectroscopy. AJNR Am J Neuroradiol 28:1517–1522

Wattjes MP, Harzheim M, Lutterbey GG, Bogdanow M, Schild HH, Traber F (2008) High field MR imaging and 1H-MR spectroscopy in clinically isolated syndromes suggestive of multiple sclerosis: correlation between metabolic alterations and diagnostic MR imaging criteria. J Neurol 255:56–63